



**HAL**  
open science

# What we can learn from crystals about the mechanical properties of glass

Tanguy Rouxel

► **To cite this version:**

Tanguy Rouxel. What we can learn from crystals about the mechanical properties of glass. Journal of the Ceramic Society of Japan, 2022, 130 (8), pp.519-530. 10.2109/jcersj2.22067 . hal-03772470

**HAL Id: hal-03772470**

**<https://hal.science/hal-03772470>**

Submitted on 8 Sep 2022

**HAL** is a multi-disciplinary open access archive for the deposit and dissemination of scientific research documents, whether they are published or not. The documents may come from teaching and research institutions in France or abroad, or from public or private research centers.

L'archive ouverte pluridisciplinaire **HAL**, est destinée au dépôt et à la diffusion de documents scientifiques de niveau recherche, publiés ou non, émanant des établissements d'enseignement et de recherche français ou étrangers, des laboratoires publics ou privés.



Distributed under a Creative Commons Attribution 4.0 International License

## REVIEW

# What we can learn from crystals about the mechanical properties of glass

Tanguy Rouxel<sup>1,2,†</sup><sup>1</sup>Glasses and Mechanics Lab., Physics Institute (IPR), UMR URI-CNRS 6251, Université de Rennes, Campus de Beaulieu, 35042 Rennes cedex<sup>2</sup>Institut Universitaire de France

Glasses and crystals from the same chemical system mostly share the same interatomic bond strength. Nevertheless, they differ by the arrangement of bonds in space, which gives birth to different atomic packing efficiencies. We show in this review that as far as the elastic moduli and hardness are concerned, the atomic packing density predominates over the bond strength. The shear modulus of a glass is usually much smaller than the one of the crystallized polymorphs, thanks to a more efficient packing of atoms in the latter. In contrast, the increase in hardness is quite limited, likely because of the additional contribution of dislocation activity to the deformation processes beneath the indenter in the case of crystals (shear plasticity). We also show that the occurrence of chemical heterogeneities (weak channels) at the mesoscopic scale in glasses, which is often associated with the lack of long range atomic ordering, promotes easy fracture paths and is responsible for the low toughness and fracture surface energy.

©2022 The Ceramic Society of Japan. All rights reserved.

Key-words : Elastic moduli, Hardness, Glass, Indentation

[Received April 26, 2022; Accepted May 13, 2022]

## 1. Introduction

In comparison to crystallized materials, glasses are generally distinguished by a better transparency (but metallic glasses of course), smaller thermal and electrical conductivities, a more brittle behavior, a worse resistance against surface damage by indentation or scratching, and the lack of permanent deformation at ambient temperature (but under a sharp contact loading). In addition, glasses are usually significantly less stiff and softer (to a lesser extent though) than their crystalline counterparts.

In this paper, the peculiarities of the mechanical behavior of glass are addressed in the light of known fundamental differences between glasses and crystals, from the atomic scale and to the microstructural one, taking examples throughout the various glass-forming chemical systems, including oxides, oxynitrides, oxycarbides, chalcogenides and metallic glasses. Each chemical system brings some pieces to the puzzle of the global picture. For instance, compositional effects within silicate glasses shed light on the key role of the atomic packing density, and those within chalcogenide glasses reflect the importance of the average atomic network cross-linking, while metallic

glasses, in comparison with oxide and chalcogenide ones, show what is going on when the interatomic bonds are losing their directionality and their topological constraints.

The relevant structural characteristics, at the atomic scale, are first introduced and discussed in connection with the elastic behavior. Those include the nature of the structural units (chains, triangles, tetrahedra, etc.), the coordination number, and the atomic packing density. Hardness is then introduced from the viewpoint of the permanent deformation mechanisms occurring at high pressure (hardness number order). The problem of crack initiation is further described on the basis of our current understanding of the ways a glassy material accommodates singular stresses, and crack extension is analyzed accounting for the details of the crack path and for the atomic organization.

## 2. Atomic organization and elastic properties

### 2.1 The structural units

In order to investigate the way the atomic-scale structural units affect the mechanical properties, let us briefly recall some results that were obtained in the framework of the topological constraint theory,<sup>1)-3)</sup> a theory that was inspired by the Maxwell stability criterion for articulated systems,<sup>4)</sup> which found some successful developments in the field of glass science. According to Maxwell criterion, a system of  $b$  articulated rigid bars consisting of  $j$  junctions (nodes) is just stable, or isostatic, when  $b = 3j - 6$  (**Fig. 1**). The basis of this equation is that each junction

<sup>†</sup> Corresponding author: T. Rouxel; E-mail: [tanguy.rouxel@univ-rennes1.fr](mailto:tanguy.rouxel@univ-rennes1.fr)

<sup>‡</sup> Preface for this article: DOI <http://doi.org/10.2109/jcersj2.130.P8-1>

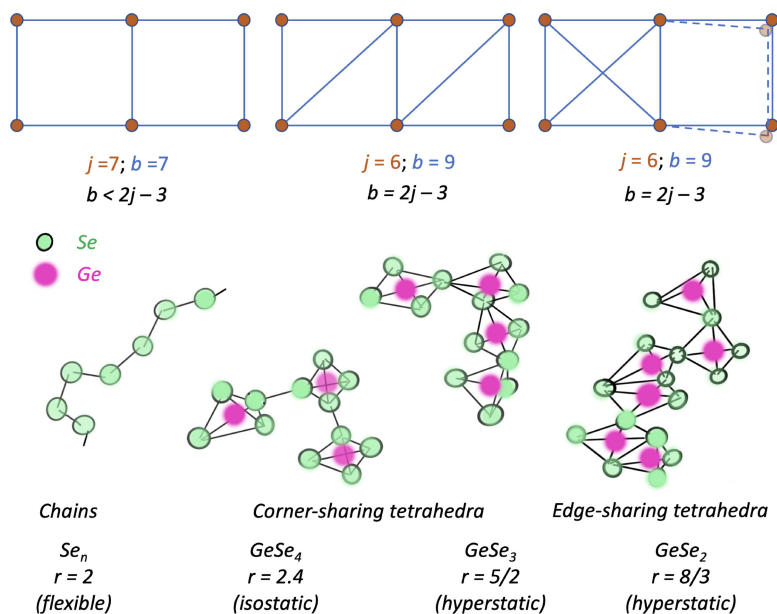


**Fig. 1.** Top: Systems of articulated bars where the degree of mobility can be calculated from Maxwell's equation. The limit of the approach is shown in the case where the system should be just stable but experiences some internal degree of freedom (floppy mode) (right). Bottom: Different glassy compounds from the (Ge,Se) system. The average coordination number is expressed as  $\langle r \rangle = 4x + 2(1 - x)$ , where  $x$  is the atomic fraction of germanium ( $Ge_xSe_{1-x}$  compound).

brings 3 possibilities for translation while the overall system, as a whole, is free to translate in the three directions of the coordinate system and to rotate around each axis, so that three « rigid body » movements are permitted. One bar suppresses one degree of internal freedom, so that the number of bars should be at least equal to  $3j - 6$  to meet stability. This reasoning was transposed to an atomic network by Philips<sup>2)</sup> and Thorpe,<sup>3)</sup> substituting bars and junctions for interatomic bonds and atoms respectively. In this latter case, there are two types of constraints, namely, the interatomic distance  $r_{ij}$ , and the dihedral angles formed by three atoms,  $\theta_{ijk}$ . Then, ignoring any possible discrete floppy modes (which may occur in the Maxwellian articulated systems as well as in the actual atomic network), the stability criterion is expressed as:

$$\sum_r n_r [r/2 + (2r - 3)] = 3 \sum_r n_r, \quad (1)$$

where  $n_r$  is the fraction of  $r$ -fold coordinated atoms. When the average coordination number,  $\langle r \rangle$ , is considered, Eq. (1) can be rewritten as:

$$\langle r \rangle / 2 + (2\langle r \rangle - 3) = 3, \quad (2)$$

where the left member gives the number of constraints (i.e.  $\langle r \rangle / 2$  distances and  $2\langle r \rangle - 3$  angles), and the right one is the degree of freedom (3 rigid body translations). Therefore, stability is just achieved for:  $\langle r \rangle = 2,4$  (Fig. 1), which, in the case of glasses from the (Ge,Se) system corresponds to the  $GeSe_4$  composition. When  $\langle r \rangle$  is larger than 2.4, the system is said to be over-constrained and might not resist crystallization. This situation is also encountered in silicon oxynitride glasses, in which three-fold coordinated nitrogen atoms substitute for two-fold oxygen

ones. When the amount of nitrogen gets as high as 5 at.%, crystallization can hardly be avoided. In the (Ge,Se) glass system, when  $\langle r \rangle$  is smaller than 2.4,  $(-Se-)_n$  chain segments are likely to form and this results in a more flexible network weakly opposing to local inter-unit sliding. A direct consequence is that as the average coordination number is decreased, shear becomes easier with respect to volume change, both in the elastic and in the flow regimes, so that the ratio of the shear modulus over the bulk one,  $\mu/K$  decreases, and Poisson's ratio,  $\nu$ , increases (Fig. 2). Let us recall that  $\nu$  is defined as the opposite of the ratio of the transverse contraction ( $\varepsilon_t$ ) to the longitudinal strain ( $\varepsilon_l$ ) in a uniaxial loading experiment:  $\nu = -\varepsilon_t/\varepsilon_l$ . It is noteworthy that the atomic network cross-linking degree is mostly correlated to the network dimensionality, that is whether the network is built on 1D chain, 2D sheet, or 3D units such as tetrahedra. For example, amorphous selenium forms chains (1D structures) whereas amorphous silica ( $a-SiO_2$ ) is chiefly 3D, like most crystals. Metasilicates (two alkaline atoms or one alkaline earth atom per Si-based tetrahedron) and phyllosilicates (one non-bridging oxygen atom per tetrahedron) lead to 1D and 2D units respectively. The distinct symbols in Fig. 2 show that there are monotonic and nearly linear decreases of  $\nu$  as  $\langle r \rangle$  or  $\langle n_{BO} \rangle$  is increased for each separate chemical systems, while the dimensionality is increased too.

This analysis is obviously questionable as soon as the interatomic bonds become weaker and less directional than in the chalcogenide systems. In the case of ionic or metallic glasses, the angular constraints are no longer decisive (or strong) and bonds can no longer be assimilated to cylindrical tubes, as in the Bohr model for atoms in cova-

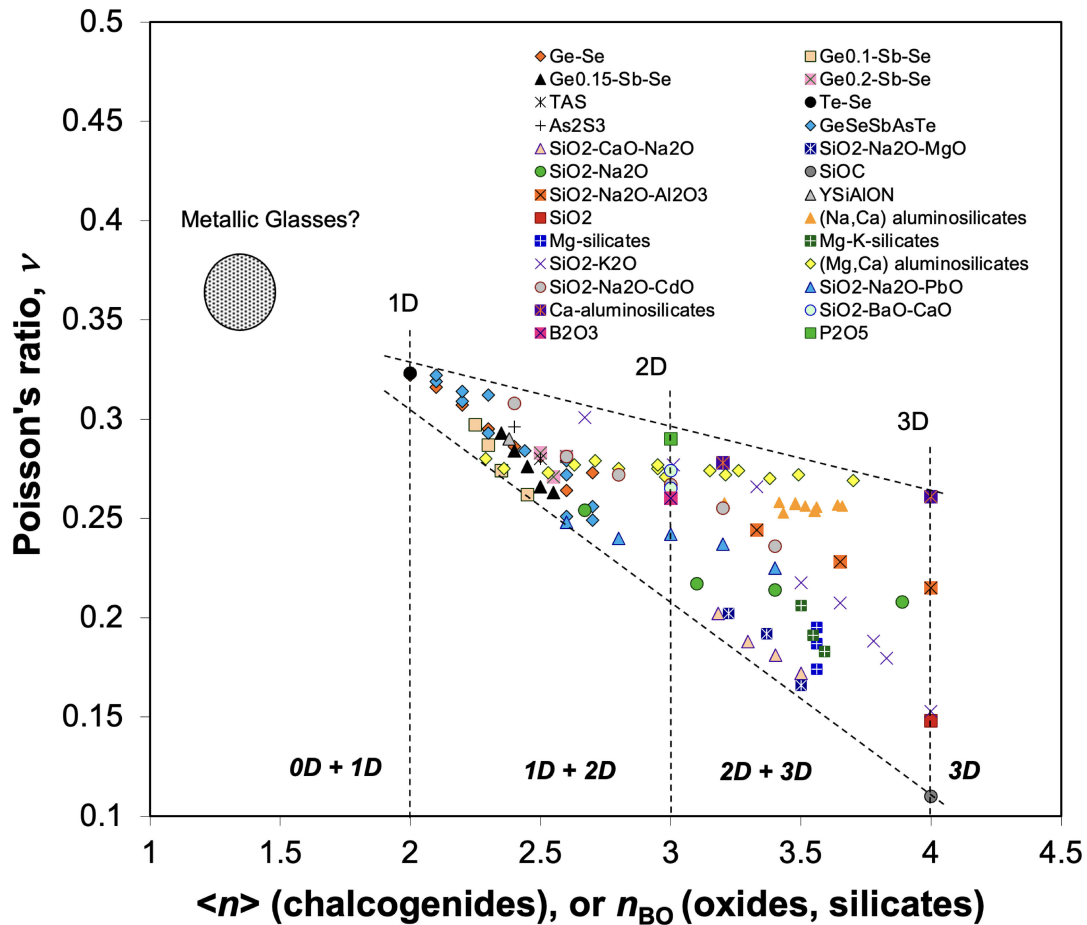


Fig. 2. Poisson's ratio ( $\nu$ ) as a function of the average coordination number  $\langle r \rangle$  or the number of bridging oxygen atoms per glass-forming cation  $n_{BO}$ . Figure reprinted with permission from Ref. 5).

lent systems. The bar/node description becomes less pertinent. For example, in the case of  $\alpha$ - $\text{SiO}_2$ , the  $\theta_{\text{SiOSi}}$  angle between two  $\text{SiO}_{4/2}$  tetrahedra spread over a relatively broad interval centered at about  $147^\circ$ , with a mid-height distribution of about  $35^\circ$ . It was thus proposed by Philips<sup>2)</sup> to remove the dihedral angle constraint (between two adjacent tetrahedra) from the stability or rigidity criterion. Then, for a glass of  $\text{Si}_x\text{O}_{1-x}$  composition, one obtains:  $x[4/2 + (2 \times 4 - 3)] + (1-x)(2/2 + 0) = 3$ , which leads to a rigidity threshold at  $x = 1/3$ . This value corresponds to the  $\text{SiO}_2$  composition, which turns out to be frequently encountered and suitable for glass formation. As an oxide,  $\text{SiO}_2$  is said to be a good glass former! Back to Maxwell criterion for articulated systems, considering a structure consisting of  $j$  junctions, then each junction may be connected to a maximum of  $j - 1$  left junctions, giving birth to an overall number of connections equal to  $j(j - 1)$ . Each bar is linked to two junctions and accounts for  $1/2$ , so that the former construction results in  $j(j - 1)/2$  bars. Such a structure is just rigid when  $j(j - 1)/2 = 3j - 6$ . There are two solutions to this equation:  $j = 3$  (triangle) and  $j = 4$  (tetrahedra). These geometrical figures are precisely the most common among glass formers in oxide systems:  $\text{BO}_{3/2}$  triangles;  $\text{BO}_{4/2}$ ,  $\text{AlO}_{4/2}$ ,  $\text{SiO}_{4/2}$  tetrahedra, etc. Nevertheless, there is no one to one relationship between

average coordination number, or the cross-linking degree, and the mechanical properties, but perhaps within a limited compositional range in a particular chemical system. For multicomponent silicate and silico-aluminate glasses, the number of bridging oxygen atoms per  $(\text{Si,Al})\text{-O}_4$  tetrahedra ( $n_{BO}$ ) can be used in lieu of the average coordination number (Fig. 2). This number can be estimated from the chemical composition, assuming for example than one alkaline and one alkaline-earth atom give birth to one and two non-bridging oxygen atoms respectively. This number is defined as:  $n_{BO} = 4 - \sum_i M_i z_i / (\sum_j F_j)$  where  $M_i$  and  $z_i$  are the atomic fraction (after deduction of the number of charge compensators) and the oxidation number of the  $i$ th modifying cation and  $F_j$  is the fraction of the  $j$ th glass-forming cation. The various series of data reported in Fig. 2 show that like what happens in a macroscopic articulated systems, the increase of the cross-linking and of the dimensionality at the atomic network scale makes the transverse contraction more difficult, so that  $\nu$  goes down as  $\langle r \rangle$  or  $\langle n_{BO} \rangle$  goes up, with a maximum Poisson's ratio value, except for metallic glasses, for chalcogen-based glasses, at  $\approx 0.34$  and a minimum value for silicon-oxy-carbide glasses, at about 0.11, where four-fold coordinated carbon atoms add to the cross-linking of the amorphous silica matrix. In the case of precious-metal (Pt, Au,

Pd, ...) based metallic glasses (MGs), the atomic packing is larger than 0.8, and  $\nu$  meets values as large as 0.4. For pure metals, the number of near neighbor atoms is equal to 8 and 12 for metals crystallizing in a body-centered and in a face-centered structure respectively. In contrast with ionocovalent glasses, where this number is controlled by the number of valence electrons, it is chiefly governed by the atomic size in metals. In such a situation, the packing density ( $C_g$ ) turns out to be a relevant parameter and, as shown in the next paragraph, there is a remarkable correlation between  $\nu$  and  $C_g$ .

As the bonding character becomes less directional and more metallic, the atomic packing efficiency comes into play. For example, the addition of 30 mol.% alkaline and alkaline-earth oxides in vitreous silica, to meet a classical composition for window glass, results in a significant decrease of the average bond strength and of the cross-linking (or average coordination number) within the atomic network. However, Young's modulus ( $E$ ) and hardness ( $H$ ) are about the same for a-SiO<sub>2</sub> and for a soda-lime-silica glass (window glass):  $E \approx 72$  GPa and  $H \approx 7$  GPa. A much larger Young's modulus ( $E > 200$  GPa) is eventually achieved in metallic glass systems, in spite of much weaker binding energies. The explanation lies chiefly in the atomic packing density, which gets better and better as the network cross-linking degree and the bond strength are decreased. As a matter of fact, it is easier to pack "hard" spheres, such as "good" metal atoms, in a box, than stiff structural units such as rods, triangles or even worse, tetrahedra!

## 2.2 The empty space

In comparison to most crystals, glasses are characterized by a less efficient atomic packing. Some significant free volume remains in the glass network, inasmuch that they were cooled rapidly (quenched) from the melting temperature. In the case of a periodic array of atoms,  $C_g$  can be determined in a straightforward manner from the geometrical characteristics of the atomic stacking, regardless of the size of the elementary cell or of the atomic radius. For cubic-centered and face-centered structures based on a single chemical element,  $C_g$  reaches values of 0.68 and 0.74 respectively. In the case of a disordered arrangement of atoms,  $C_g$  can be determined from the ratio of the effective volume occupied by a mole of atoms ( $V_a$ ), as estimated from the atomic radii ( $V_a = \mathcal{N} \sum_i 4/3\pi x_i r_i^3$ , where  $\mathcal{N}$  is Avogadro number and  $x_i$  and  $r_i$  are the atomic fraction and ionic radius of the  $i$ th element), to the corresponding volume of glass ( $V_0$ ), calculated from the specific mass of the glass ( $\rho$ ) and the molar mass of the constituents [ $V_0 = (1/\rho) \sum_i x_i m_i$ , where  $m_i$  is the molar mass of the  $i$ th element]:

$$C_g = \frac{\mathcal{N} \sum_i (4/3)\pi x_i r_i^3}{(\sum_i x_i m_i) / \rho} \quad (3)$$

In multicomponent systems where atoms are relatively free to explore the empty space of the atomic network, large  $C_g$  values may be obtained. This situation is observed

in metallic glasses based on precious metals, which exhibit  $C_g$  values as large as 0.8. In the case of silicate glasses,  $C_g$  ranges typically between 0.45 and 0.55 (Fig. 3).<sup>6-8)</sup> The correlation between  $\nu$  and  $C_g$  stands regardless of the order versus disorder character of the atomic organization. Nevertheless, it can be seen in Fig. 3 that elements crystallizing in the same structure, that is with the same theoretical packing density, may exhibit different  $\nu$  values. This is because as the atomic number increases, bonds tend to become less directional and shear sliding becomes easier, resulting in a more isochoric deformation. For example,  $\nu_{\text{diamond}} < \nu_{\text{Si}} < \nu_{\text{Ge}}$  for cubic diamond structure and  $\nu_{\text{Be}} < \nu_{\text{Pb}}$  for the face-centered cubic structure.

Let us consider the case of vitreous silica. The bulk modulus ( $K$ ) of a-SiO<sub>2</sub> is equal to 33 GPa. The addition of 30 mol.% of a mixture of alkaline ( $A$ ) and alkaline-earth ( $AE$ ) oxides (Na<sub>2</sub>O, K<sub>2</sub>O, MgO, CaO) leads to a value of 44 GPa for  $K$ , that is a larger value in spite of much smaller bond energies for the added constituents:  $U_{0(\text{Na-O})} = 73$  kJ.mol<sup>-1</sup>,  $U_{0(\text{K-O})} = 49$  kJ.mol<sup>-1</sup>,  $U_{0(\text{Mg-O})} = 166$  kJ.mol<sup>-1</sup>, and  $U_{0(\text{Ca-O})} = 177$  kJ.mol<sup>-1</sup>, whereas  $U_{0(\text{Si-O})} = 624$  kJ.mol<sup>-1</sup>.<sup>9)</sup> However,  $C_g$  is increased in the presence of  $A$  and  $AE$  oxides, to about 0.516 for a standard window glass, while it is as small as 0.454 for a-SiO<sub>2</sub>. This is a clear evidence for the role played by  $C_g$  on the elastic moduli. An explicit relationship between  $K$  and the interatomic bond energy is expressed by the 1st Grüneisen rule,  $K = mn|U_0|/(9V_0)$ , where  $m$  and  $n$  are the exponents of the pair potential, [ $U(r) = A/r^m - B/r^n$ ],  $U_0$ , is the bond energy and  $V_0$  is the molar volume (provided  $U_0$  is given in J.mol<sup>-1</sup>). This expression can be extended to a complex glass composition using the average dissociation enthalpy ( $\langle U_0 \rangle$ ) and volume ( $\langle V_0 \rangle$ ) of an equivalent mole of glass (also referred to as a *gram-atom*). As long as the bonds are assumed to be similar in a glass and in a crystal having the same stoichiometric formula, then the ratio of the bulk modulus of the glass to the one of the crystal is given by:  $K_g/K_c = V_{0c}/V_{0g}$ , and with the densities,

$$K_g/K_c = \rho_g/\rho_c, \quad (4)$$

or alternatively, with the atomic packing density:

$$K_g/K_c = C_{g,g}/C_{g,c} \quad (5)$$

For example, the density of  $\alpha$  quartz, an allotropic variety (or a polymorph) of a-SiO<sub>2</sub>, is equal to 2.65 g.cm<sup>-3</sup> and is greater than the one of a-SiO<sub>2</sub> (2.2 g.cm<sup>-3</sup>). The isothermal bulk modulus of quartz is equal to 38 GPa, whereas the one of a-SiO<sub>2</sub> is equal to 33 GPa, so that  $K_g/K_c = 0.87$ , which is close to the density ratio: 0.83. However, as the crystallized phase used to estimate the glass properties becomes more efficiently packed,  $K_g/K_c$  becomes much smaller than  $\rho_g/\rho_c$ . For example, in the case of stishovite, another allotropic variety of SiO<sub>2</sub> but where Si is six-fold coordinated,  $K_g/K_c = 0.11$  ( $K_{\text{stishovite}} \approx 295$  GPa),<sup>10)</sup> whereas  $\rho_g/\rho_c = 0.515$ . In a detailed investigation of the correlation between the bulk modulus and the atomic packing density of silicate glasses and their crystallized polymorphs (in particular MgSiO<sub>3</sub>, CaMgSi<sub>2</sub>O<sub>6</sub>

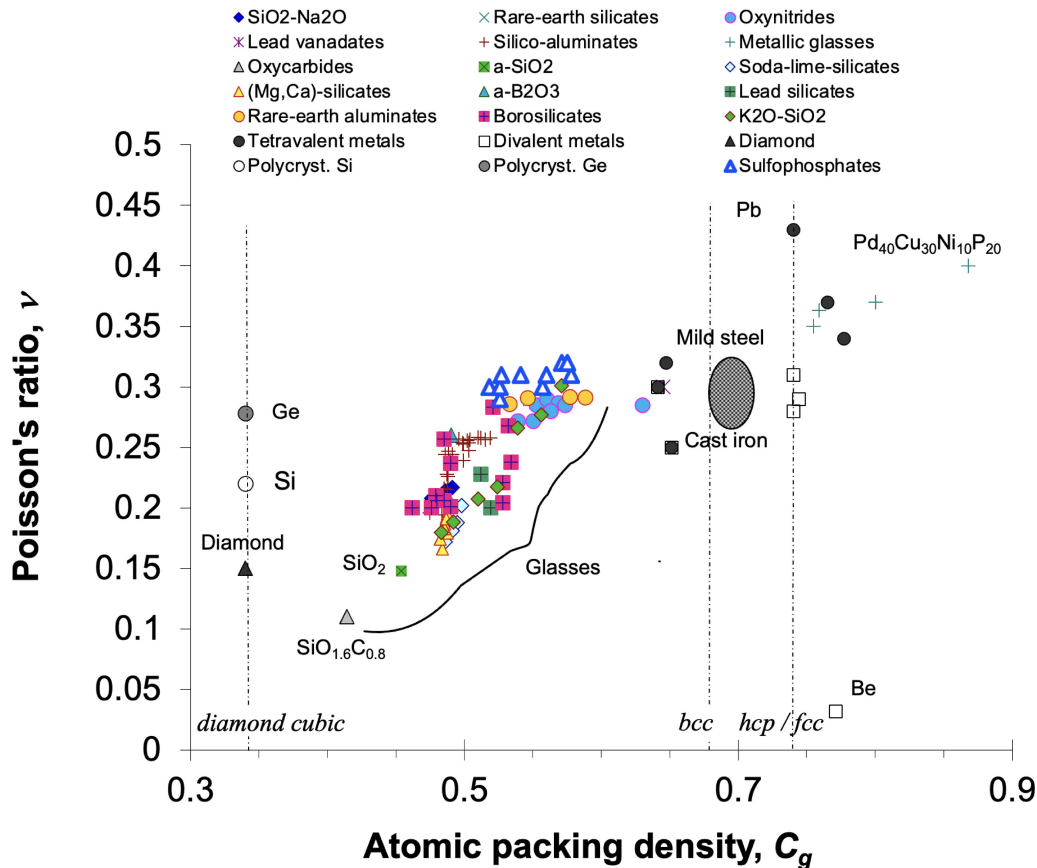


Fig. 3. Poisson's ratio,  $\nu$ , as a function of the atomic packing density,  $C_g$ . The distinct symbols show that there are monotonic increases of  $\nu$  with  $C_g$  for each separate chemical system. Figure adapted with permission from Ref. 6) and augmented with data from alkali-borosilicate<sup>7)</sup> and sulfophosphate<sup>8)</sup> glasses.

and  $\text{SiO}_2$  compounds), it was found that although  $K$  depends almost nearly on  $C_g$ , the slope changes from one chemical system to the other and there is a threshold value for  $C_g$  below which  $K$  tends toward zero.<sup>11)</sup> This critical value is close to 0.45. This discrepancy may be attributed to an increase of the  $mn$  product in the pair potential with  $C_g$  since the interatomic potential well becomes steeper as the density is increased, especially for the high-pressure phases such as stishovite (or coesite), and also to a lesser extent to a change in the dissociation enthalpy, and in the atomic radii. There are indeed many cases of elements and compounds exhibiting a more metallic behavior (i.e. a decrease in bond charge) under pressure,<sup>12),13)</sup> such as hydrogen becoming metallic, or semi-conductors becoming conductors.<sup>12)</sup> Although there is no general rule and the high pressure behavior can hardly be predicted, this suggests a change in the bond character, and an increase of  $m$  with the density, or as the atomic packing gets closer to the hard spheres model. Further in-depth atomistic investigations are required to clarify this point.

This reasoning was successfully applied to find the elastic modulus of relatively simple glasses for which the stoichiometry could be ascribed to a combination of different crystallized phases. For an arbitrary glass composition (that is with little hope to find a crystallized polymorph),  $\langle U_0 \rangle$  can be estimated from the dissociation enthalpy of

each oxide ( $A_xO_y$ ) introduced in the composition,<sup>5),14)</sup>  $\Delta H_d$ , which is given by a classical Born-Haber cycle:  $\Delta H_d = -\Delta H_f(A_xO_y) + x\Delta H_{at}(A) + y\Delta H_{at}(O)$ , where  $\Delta H_f$  is an enthalpy of formation and  $\Delta H_{at}$  is an atomization enthalpy, and for the diatomic oxygen molecule,  $\Delta H_{at}(O; 1/2 O_2 \rightarrow O_g) = 249,18 \text{ kJ}\cdot\text{mol}^{-1}$ . Let's consider a glass obtained by melting of a mixture of 30 mol.% BaO, 30 mol.%  $\text{TiO}_2$  and 40 mol.%  $\text{SiO}_2$ . The dissociation enthalpy for  $\text{SiO}_2$  is given by:  $\Delta H_d(\text{SiO}_2) = -\Delta H_f(\text{SiO}_2) + \Delta H_{at}(\text{Si}) + 2\Delta H_{at}(\text{O})$ . This gives:  $\Delta H_d(\text{SiO}_2) = 910.7 + 450 + 2 \times 249.2 = 1859 \text{ kJ}\cdot\text{mol}^{-1}$ . In a similar way, we obtain 976 and 1915  $\text{kJ}\cdot\text{mol}^{-1}$  respectively for BaO and  $\text{TiO}_2$ . Therefore, after weighting these values according to the molar fraction of each oxide, one obtains  $\langle U_0 \rangle = 1611 \text{ kJ}\cdot\text{mol}^{-1}$  for the glass (or  $604 \text{ kJ}\cdot\text{mol}^{-1}$  for the equivalent gram-atom, which writes:  $\text{Si}_{0.15}\text{Ba}_{0.11}\text{Ti}_{0.11}\text{O}_{0.63}$ ). The specific mass of this glass is equal to  $4,02 \text{ g}\cdot\text{cm}^{-3}$  and the molar mass, expressed as  $\sum_i f_i m_i = 0,4m_{\text{Si}} + 0,3m_{\text{Ti}} + 0,3m_{\text{Ba}} + 1,7m_{\text{O}}$ , is equal to 94 g, which gives a molar volume  $\langle V_0 \rangle = 23.4 \text{ cm}^3$ . Therefore  $\langle U_0 \rangle / \langle V_0 \rangle = 68.8 \text{ GPa}$ , which is in agreement with the experimental value of 70.1 GPa. This suggests that, at least for oxide glasses, the  $mn$  product of the pair potential is close to 9. Nevertheless, the agreement between the theoretical prediction and the experimental data is generally not that good, not only because the atomic bonding character is not well known in complex systems, but also

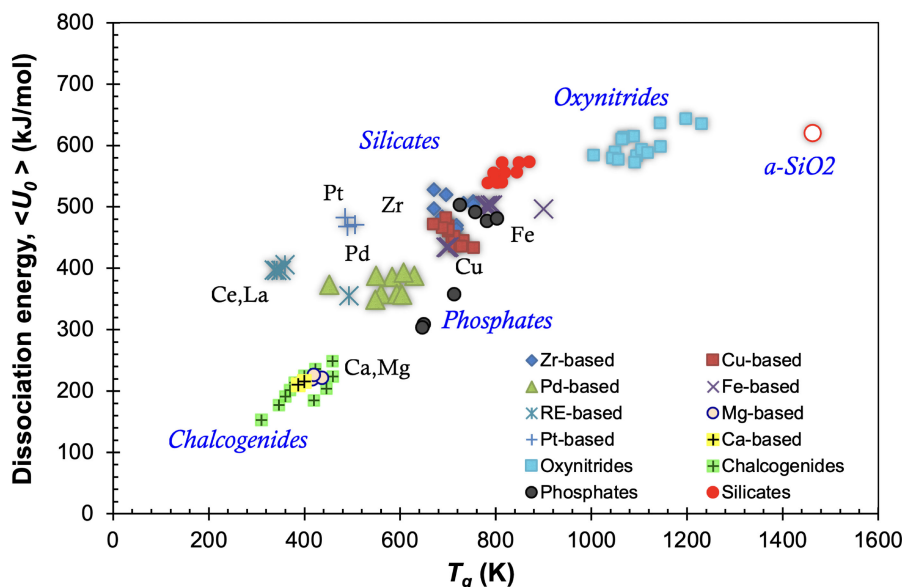


Fig. 4. The dissociation energy ( $\langle U_0 \rangle$ ) for a gram-atom of glass, as estimated from thermochemistry data as a function of  $T_g$ . Figure reprinted with permission from Ref. 15).

because there are fundamental issues with the determination of  $C_g$ , such as the chosen values for  $r_i$  (which depend on the oxidation number, on the coordination, etc.), provided invoking atom radius remains meaningful. It is noteworthy that in the same way that the binding energy of crystals scales with their melting point, the average dissociation energy of glasses scales with  $T_g$  (Fig. 4).<sup>15)</sup> In Fig. 4, the energy content ( $\langle U_0 \rangle$ ) of MGs was estimated from the atomization enthalpies of the single elements and from the enthalpy of mixing (usually negligible in comparison to the atomization enthalpies). The mean dissociation enthalpy ranges from about 100 kJ.mol<sup>-1</sup> for chalcogenide glasses to 700 kJ.mol<sup>-1</sup> for silicon-oxynitride glasses. It follows that the shear modulus of glass evolves more or less like the glass transition temperature, and that hardness, which was found to scale with  $\mu$  in many crystallized systems is also more or less scaling with  $T_m$  for crystals and with  $T_g$  for glasses. But these are rough approximations (see Fig. 2 in Ref. 16)) since, on the one hand, the atomic packing factor is ignored, on the other different mechanisms may result in the same hardness number, as is discussed in the next paragraph. Besides, elastic moduli and hardness are given in Pa, that is in J.m<sup>-3</sup>, whereas a temperature has the dimension of an energy.

### 2.3 Hardness

The hardness of glasses containing a large free volume content, such as vitreous silica (a-SiO<sub>2</sub>), is predominantly controlled by the volume density of atomic bonds, regardless of the interatomic bond energy. This is the reason behind a-SiO<sub>2</sub> ( $H = 8.7$  GPa) being considerably softer than its crystalline counterparts, quartz ( $H = 10\text{--}12$  GPa), coesite ( $H \approx 10$  GPa) or than its high-density variant, the stishovite ( $H \approx 33$  GPa).<sup>17),18)</sup> With an increase in the packing density, the bond strength becomes more dominant than the packing density itself, and the resistance offered by the

glass to the shear flow governs hardness. This is why MGs, which have a remarkably large atomic packing density, which reflects in their Poisson's ratios being typically larger than 0.3, can be stiffer than - and as hard as - oxide glasses, despite much weaker interatomic bonding.

Typical  $H$  values for inorganic, non-metallic glasses range between 1 (chalcogenides) and 12 (silicon-oxynitrides) GPa. These are obviously much larger than the stresses that glasses can withstand during ordinary mechanical testing (such as uniaxial tension or compression tests) or in service conditions, and are sufficient to generate some densification in the process zone beneath the imprint. Densification at indentation sites was deduced from changes in the refractive index as measured by optical interferometry,<sup>19),20)</sup> as well as by Raman spectroscopy,<sup>21),22)</sup> and was recognized to be a general property of glasses. Densification, which is a displacive transformation, shows up through a persistent change of the atomic network structure in the region that extends up to several times the indentation size beneath the surface, and involves a collapse of matter into a relatively-more close packed structure. The extent to which a glass can densify during indentation depends on its atomic packing density. The smaller  $C_g$  is, and the larger the magnitude of the volume shrinkage becomes. In the case of amorphous silica (a-SiO<sub>2</sub>), densification accounts for 80 % of the indentation volume, whereas for a Zr-based metallic glasses, which has a random close packed structure, it contributes to less than 10 % of the deformed volume.<sup>22)</sup> Beside densification, the other major contribution to the formation of an imprint is the isochoric and shear-driven flow of matter. Densification occurs first, in an axisymmetrical blister-shape like region extending to a depth scaling with the indentation size, while shear flow relays on and is very much localized along the contact area, eventually resulting in some piling-up of material at the vicinity of the imprint.<sup>23)</sup>

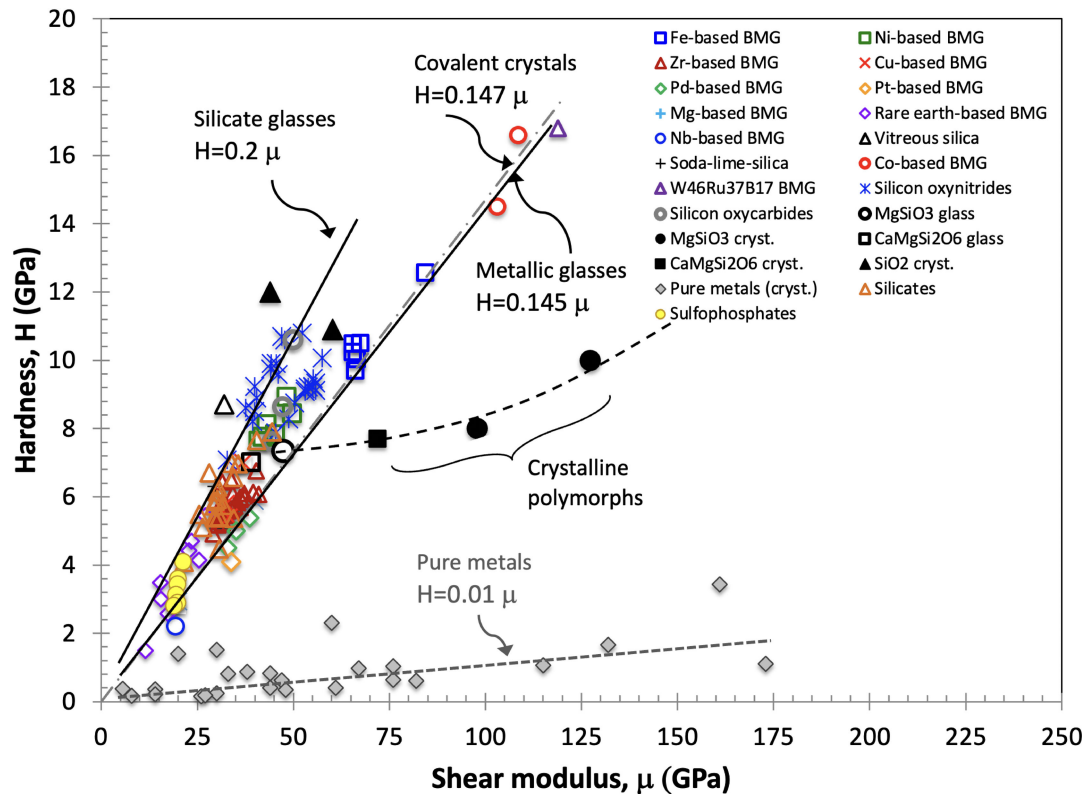


Fig. 5. The hardness–shear modulus correlation. The bold straight lines correspond to the best linear fitting for bulk metallic glasses (data from Ref. 24)) and for silicate glasses (data from Refs. 16) and 29)). Data on glass crystallized polymorphs and metamorphic minerals were taken from Refs. 17) and 18). Data on chalcogenide, oxynitride and oxycarbide glasses were extracted from Refs. 25), 26), 27) and 28) respectively. The linear correlation observed for covalent crystals is from Ref. 30).

In the case of crystalline materials, and especially metals, the residual indentation print can be attributed to the movement of dislocation and is chiefly correlated to the shear modulus (per the Peierls expression for the lattice friction force), and to a lesser extent to some diffusion processes (especially at elevated temperature) when the transport of matter plays a role in the permanent deformation, as in the cases of dislocation climb or diffusion creep for example. Therefore, hardness values are typically below 3 GPa for metals, and  $H$  is proportional to the macroscopic flow stress and to the shear modulus:  $H \approx 0.01\mu$  (Fig. 5). *MGs*, which deform by localized shear-transformation-zone processes,<sup>24)</sup> are mostly hard ( $H$  ranges between 2 and 18 GPa) and exhibit a much larger slope:  $H \approx 0.145\mu$ , close to the one observed for covalent crystals,  $H \approx 0.147\mu$ ,<sup>30)</sup> but smaller than the one for silicate glasses,  $H \approx 0.2\mu$ . The differences observed between these classes of materials derive from the fundamental changes in the deformation mechanism and is discussed below.

The possible and eventually concomitant mechanisms resulting in a permanent imprint at the surface of glass in ambient conditions include i) densification; ii) isochoric shear flow; and iii) damage-based processes (microcracking). Furthermore, the shear deformation processes, which are reconstructive by nature, may greatly differ depending on the material. Shear-thinning viscous flow, where the non-linear rheological behavior stems from the high pres-

sure that builds at indentation site, can be invoked for non-metallic glasses. In the case of *MGs*, the fundamental unit processes of deformation occur via the collective shuffling of clusters of atoms to accommodate the applied shear strain. These are termed “shear transformation zones” (*STZs*), and result in an inhomogeneous plastic flow into narrow shear bands with typical thickness of  $\sim 10$  nm.<sup>24)</sup> These shear bands, after propagating through a characteristic distance, become shear cracks. The absence of dislocations in *MGs*, however, makes them considerably harder than their crystalline counterparts. Interestingly, the occurrence of dislocation activity in crystalline polymorphs of silicate glasses (bold marks in Fig. 5) prevents from a significant increase of hardness in these polymorphs in comparison with the parent glass, in spite of a dramatic increase of the shear modulus. Dislocation glide was observed in  $\text{MgSiO}_3$  (bridgmanite), having a perovskite-type structure, with  $[100](010)$  and  $[010](100)$  slip systems,<sup>31)</sup> and in  $\text{CaMgSi}_2\text{O}_6$  (diopside) at  $T < 500^\circ\text{C}$ , plastic deformation takes place by mechanical twinning on  $(100)[001]$  and  $(001)[100]$  with dislocation glide on  $(100)[001]$ ,  $(100)[010]$  and  $(010)[100]$ .<sup>32)</sup> In the case of quartz, although dislocation slip was reported and mainly takes place in the  $a$ ,  $c$  and  $\langle a+c \rangle$  directions, mostly along  $(0001)$  and  $\{10\bar{1}0\}$  planes, it turns out that glide is very limited at ambient pressure and temperature,<sup>33),34)</sup> and indeed no dislocation activity was detected at Vickers

indentation sites.<sup>35)</sup> Dislocation activity in coesite is strongly constrained by the pseudo-hexagonal symmetry and some analogies are thus found with deformation mechanisms observed in quartz. As a matter of fact, in spite of smaller shear moduli for quartz and coesite in comparison to  $\text{MgSiO}_3$  and  $\text{CaMgSi}_2\text{O}_6$  phases,  $\text{SiO}_2$  high pressure polymorphs are harder. Another important feature of the permanent deformation mechanism at indentation site is that shear flow, whatever its physical origin, is more sensitive to temperature than volumetric change, such as densification, so that densification, as long as there is enough room for it (that is the free volume content is large enough), becomes more and more important as the glass is cooled and, on the contrary, shear, as revealed by shear bands and piling-up of matter at the border of the imprint, is favored at elevated temperature.<sup>35),39)</sup> Shear phenomena in general, including elasticity, dislocation plasticity or viscosity, predominates over isobaric ones as temperature is raised, inasmuch as densification is bounded, by nature, whereas large strain can be achieved in shear, with no theoretical limit. For example,  $\mu$  decreases faster than  $K$  upon heating, so that  $\nu$  increases and the behavior becomes more volume conservative. The occurrence of dislocation activity in crystals or of viscous flow in glasses is also a direct consequence of the rapid decrease of the yield stress upon heating, so that a brittle to ductile transition is observed when this stress becomes smaller than the strength of the material at this temperature. In both cases, a shear thinning behavior is mostly observed, so that shear flow is also more and more significant as the stress (or contact pressure) is increased. The intrinsic strength of silica and silicate glasses is of the order of 14 to 20 GPa in vacuum, as shown both experimentally<sup>36)</sup> and by MD simulation.<sup>37)</sup> Since densification, which leads to a 20% density change, begins at about 10 GPa (with the first plateau being met at  $\approx 18$  GPa), densification is the major deformation contribution in a-SiO<sub>2</sub>. However, plastic flow relays on as the glass is densified.<sup>23)</sup> Plastic flow shows up in tension in densified silica glass samples, in between 10 and 15 GPa tensile stress, depending on the extent of the pre-densification treatment, suggesting that flow in amorphous silica is directly correlated to the occurrence of 5- and 6-fold coordinated silicon.<sup>37)</sup> In spite of a-SiO<sub>2</sub> failing in a brittle manner in tension at about 15 GPa in vacuum, the tensile strength of a-SiO<sub>2</sub> decreases down to 6 to 7 GPa in moisture environment<sup>36)</sup> and some more recent studies dealing with the behavior of  $\mu\text{m}$  size micropillars suggested a yield stress in compression in air for plastic flow of about 7 GPa.<sup>38)</sup> There still remains fundamental questions about the way vitreous silica permanently deforms in ambient conditions. It is known that shear promotes pressure densification and that the elastic behavior is strongly non-linear. Besides elastic moduli changes in a complicated manner with pressure.

The fundamental reason for the lack of a one to one relationship between  $H$  and  $\mu$  (Fig. 5) is that whereas  $\mu$  can be seen as a bulk material property, reflecting the energy content per unit volume in the material, or in other words

the arrangement of bonds in space, hardness accounts for some fine heterogeneous details of the atomic organization, such as the presence of easy shear paths (slip planes for crystals, weak channels in glass).

The permanent deformation in glasses is reflected in  $\nu$ . As a matter of fact, in the same way that  $\nu$  of crystalline polymorphs increases with the density ( $\nu_{\text{quartz}} = 0.09$ ,  $\nu_{\text{coesite}} \approx 0.18$ ,  $\nu_{\text{stishovite}} = 0.22$ ),<sup>39),40)</sup>  $\nu$  increases in glasses under pressure (from 0.15 to 0.33 in a-SiO<sub>2</sub>)<sup>41)</sup> as well as after permanent densification.<sup>23)</sup> As  $\nu$  increases, isochoric shear relays on densification under a sharp contact loading. Furthermore, as shear deformation becomes easier relative to the volume change,  $H$  decreases and  $E/H$  increases, as well as  $E/\mu$  and  $K/\mu$ . Since both  $E/\mu$  and  $K/\mu$  scale with  $\nu$ , it turns out that examining  $E/H$  or  $\nu$  to anticipate sink-in or pile-up is about the same thing.<sup>42)</sup> Note that ductile materials, which show extensive pile-up, are comparatively soft and exhibit large  $\nu$  values (and large  $C_g$  ones). Nevertheless, even in the cases where volume conservative flow is the dominant mechanism, the pile-up volume remains noticeably smaller than the indentation volume. It represents 34, 61, and 75% of the volume of the imprint for a  $\text{Zr}_{55}\text{Cu}_{30}\text{Ni}_{10}\text{Al}_5$  MG,  $\text{GeSe}_4$  glass, and pure crystalline platinum, respectively.<sup>23)</sup> This is because a significant fraction of material moves downwards into the bulk, inducing post-unloading residual stresses. Such stress field prevents against a complete recovery of the elastic energy stored during the loading stage and is responsible for the radial-median cracks observed at higher loads in brittle solids and discussed in the next paragraph.

### 3. Cracking

#### 3.1 The crack formation process

Surface damage by indentation or scratching is a major issue in glass industry, in architecture, or for the life durability of flat displays. On the one hand, it alters the optical properties, including transparency and visual aspect, and on the other hand, it significantly decreases the strength and the safety of glass products. It also raises fundamental scientific questions, such as how glass permanently deforms under a sharp contact loading and whether there is anything to be done to reduce glass brittleness? Sharp contact loading experiments, by means of cube-corner, Vickers, Knoop or Berkovich indenters, are useful techniques to characterize the onset for crack initiation, with the aim to reproduce what may happen in service conditions when the surface of a glass part is damaged (by impacts, scratches, indents, etc.). The crack resistance of a glass can be assessed by means of Vickers indentation tests, by indenting stepwise at increasing loads, and counting the number of radial cracks emanating from the corners of the residual imprints.<sup>43)</sup> The probability of crack initiation is then defined as the ratio between the number of corners where a radial crack was formed and the total number of corners (4 for a Vickers test). When the occurrence of two radial cracks (optical microscope resolution) from two opposite corners of a Vickers indent (four cracks are observed when the indentation cracking pattern is fully

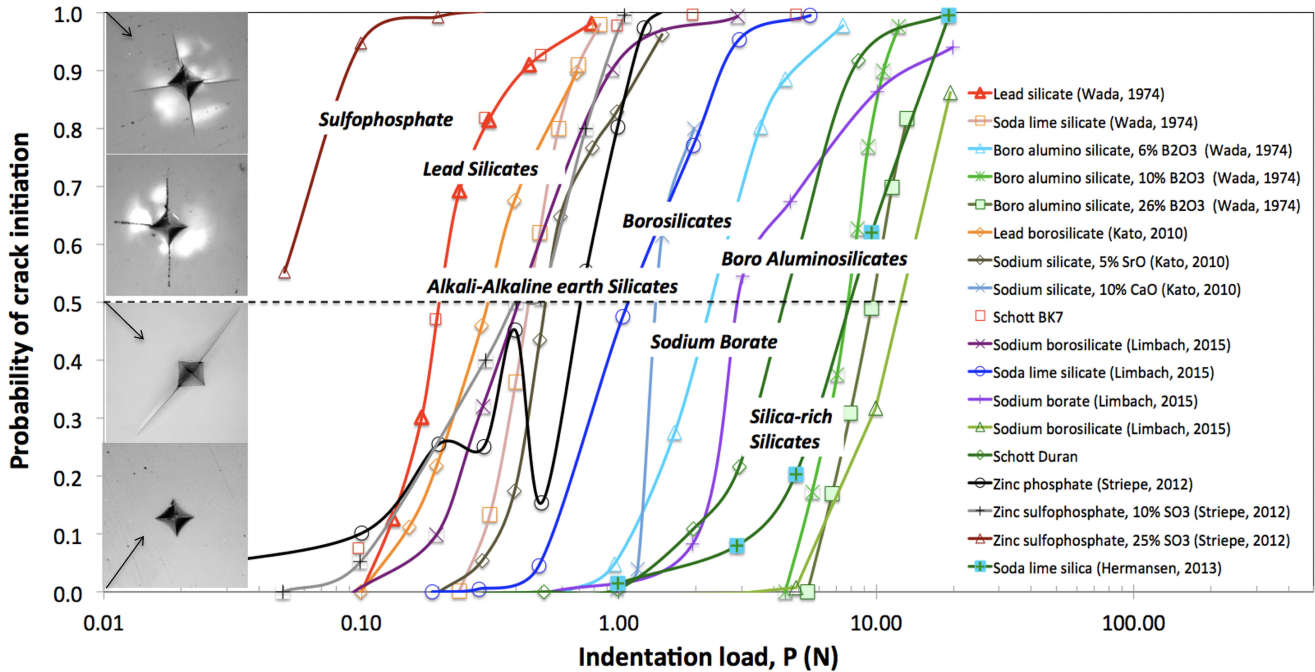


Fig. 6. The probability of crack initiation at different applied loads. The probability is determined as the average number of radial cracks per corner out of a series of Vickers indents (typically over 10) performed at a given load. The crack resistance is the load where the probability of crack initiation is equal to 50 % (i.e. two corners out of four exhibit cracks on average). Insets on the left show typical indentation cracking patterns corresponding to 0, 2, 3 and 4 well developed radial cracks. Reprinted with permission and adapted from Ref. 16).

developed) is considered as a criterion for the onset of indentation cracking, values of  $\sim 0.3$ ,  $0.7$ ,  $1$  and  $10$  N are obtained for the critical indentation load for lead glasses, window glasses, *E*-glass (a low alkali boro-aluminosilicate glass) and the mother Vycor glass [silica-rich (96 mol.%) borosilicate glass] respectively (Fig. 6).

There is no one to one relation between the onset load for crack initiation and mechanical properties such as  $H$ , fracture toughness ( $K_{Ic}$ ), elastic moduli, strength, or any simple combination of those such as the brittleness index ( $B = H/K_{Ic}$ )<sup>29),42),44),45)</sup> but with the ability of the glass to experience densification beneath the indentation zone.<sup>16),43),45),46)</sup> The general trend, again confirming the crucial role of  $C_g$ , is that glasses with relatively open atomic structures, such as  $\alpha$ - $\text{SiO}_2$ , are more resistant toward crack initiation than glasses with large atomic packing density, such as lead-borate glasses for example,<sup>16),47)</sup> and indeed an increase in the critical crack initiation load with the densification contribution to the formation of the imprint (and thus with the decrease of the intensity of the residual stress field) was found.

### 3.2 Crack propagation: fracture toughness and fracture surface energy

Fracture toughness ( $K_{Ic}$ ) and fracture surface energy ( $\gamma$ ) values as obtained by standard notched-beam specimens where the crack depth is known (the crack is assimilated to the notch, eventually with the addition of some length due to fatigue crack growth) and the stress at fracture is measured, are often greatly overestimated due to different

energy dissipation processes operating at the vicinity of the crack front. Besides, in most cases, the elastic energy stored both in the specimen and in the testing machine at the onset of crack extension is large enough to cause a catastrophic, unstable fracture, especially when it is realized that  $\gamma$  is typically smaller than  $1 \text{ J}\cdot\text{m}^{-2}$  for glasses. This situation prevents from a straightforward measurement of the fracture surface energy from the area under the load-displacement curve. Nevertheless, there are few suitable experimental methods, among which the chevron-notch beam (CN), the controlled-surface flaw (CSF), and the single-edge precracked beam (SEPB) ones,<sup>48)</sup> allowing for the determination of  $\gamma$  either from the mechanical work (load  $P$ ; displacement  $u$ ) associated with the stable (quasi-static) fracture process:

$$\gamma = \left( \frac{1}{2S} \right) \int_0^{u_r} P(u) du \quad (6)$$

where  $S$  is the area of the fracture surface and coefficient 2 in the right member accounts for the two walls of the fracture surface, or from the onset for crack initiation using the Irwin-Griffith similarity principle:

$$\gamma = \frac{K_{Ic}^2}{2E'} \quad (7)$$

where  $E' = E$  in plane stress and  $E' = E/(1 - \nu^2)$  in plane strain.

The intrinsic fracture toughness and surface energy were measured in a series of glasses with different compositions, and the agreement between  $\gamma$  values as obtained

from Eqs. (6) and (7) and support the fact that the crack tip, in such brittle materials, is atomically sharp. This finding corroborates observations made by means of *HR-TEM* and *AFM* in glasses and ceramics.<sup>49)–51)</sup>

A relatively simple approach to predict  $\gamma$  and  $K_{Ic}$  in a quantitative manner consists in assuming that a propagating crack extends following a path disrupting the weakest links of the energy landscape, and to estimate the surface energy from the bond strength and the bond concentration along this fracture surface. The intrinsic (or theoretical) fracture surface energy is obtained from the surface density of representative structural units and from the relevant bond strength. Let us first consider again  $\alpha$  quartz. This material usually exhibits a conchoidal fracture, which suggests that there is no preferential fracture plane (as in the case of glass), and this is indeed a common way to identify quartz in geology. Nevertheless, two easy cleavage planes were identified in the trigonal trapezoidal lattice structure of this crystallized phase, namely the (01 $\bar{1}$ 1) et (11 $\bar{2}$ 0) planes.<sup>52),53)</sup> The  $\alpha$  quartz lattice elementary cell contains a silicon oxide ring consisting of 6 oxygen atoms inside a parallelepipedic cell ( $a = 4.912 \text{ \AA}$ ,  $b = 4.912 \text{ \AA}$ ,  $c = 5.404 \text{ \AA}$ ,  $\alpha = 90^\circ$ ,  $\beta = 90^\circ$ ,  $\gamma = 120^\circ$ ) and 6/2 silicon atoms (on the faces). In the case of the prismatic (11 $\bar{2}$ 0) plane, associated with the [1 $\bar{1}$ 00] cleavage direction, the area ( $S$ ) of a plane surface cutting this cell is  $2 \times a \times c \times \cos 30^\circ$ . One finds  $S(11\bar{2}0) = 46 \text{ \AA}^2$ . In such a plane, a passing-through crack cuts two Si–O bonds. With a bond energy of  $624 \text{ kJ.mol}^{-1}$ ,<sup>9)</sup> this leads to a value of  $2 \times 624.10^3 / (\mathcal{N} \times 46.10^{-20})$  for  $\gamma$ , where  $\mathcal{N}$  is Avogadro's number. Therefore  $\gamma = 4.5 \text{ J.m}^{-2}$ , which is in agreement with the value of  $4.44 \text{ J.m}^{-2}$  that is deduced from the experimental  $K_{Ic}$  value derived from a quasi-static stable fracture test, taking Young's modulus equal to  $76 \text{ GPa}$  in the direction normal to the cleavage plane.<sup>53)</sup> This approach was successfully applied to relatively complex glass systems replacing the cleavage plane by a plane of arbitrary orientation (random) and taking the number of disrupted bonds from the stoichiometric formula (gram-atom), assuming that a crack preferentially cuts the weakest links of the network.<sup>54)</sup> Let  $x_i$  be the stoichiometric fraction of the species involved in the  $i$ th bonding energy  $U_{oi}$  (in  $\text{J.mol}^{-1}$ ), between the  $i$ th cation ( $A_i$ ) and a first neighbor oxygen anion in the case of an oxide glass, and let  $n_i$  be the number of such bonds supposed to be broken as the crack front propagates to the next unit, then  $\gamma$  is expressed as:

$$\gamma = \frac{1}{2} \left( \frac{\rho}{M_o} \right)^{2/3} \mathcal{N}^{-1/3} \sum_i x_i n_i U_{oi} \quad (8)$$

where the  $1/2$  prefactor on the right-hand side member accounts for the fact that the bond disruption process leads to the formation of two complementary surfaces.

It is noteworthy that the  $A_i$ -O bond dissociation energy in a glass network is usually not known accurately. Hence,  $U_{oi}$  was taken either as the dissociation enthalpy of the  $A_{ix}O_y$  compound,  $D^\circ(A_{ix}O_y)$ , divided by  $x$  and by the coordination number of  $A_i$  to oxygen, or as the  $A_i$ -O bond

dissociation enthalpy,  $D^\circ(A_i-B)$  or fission enthalpy. It turns out that a better correlation between experimental and theoretical  $K_{Ic}$  values is obtained with  $D^\circ(A_i-B)$ , although this latter parameter significantly overestimates the bond strength in the network. An equivalent expression to Eq. (8) is obtained with  $C_g$ :

$$\gamma = \frac{1}{2} \left( \sum_i \frac{4}{3} \pi x_i r_i^3 \right)^{-2/3} \mathcal{N}^{-1} C_g^{2/3} \langle U_o \rangle \quad (9)$$

where  $\langle U_o \rangle = \sum_i x_i n_i U_{oi}$  is the mean energy content in a gram-atom of glass.

The fracture surface energy of glass can also be estimated from the one of an allotropic crystal (when such a material exists), considering that the volume density of energy scales with the specific mass ( $\rho$ ), and further that the surface density of energy is proportionnal to  $\rho^{2/3}$ . Then, for the glass:

$$\gamma_{\text{ver}} = \gamma_{\text{crist}} (\rho_{\text{ver}} / \rho_{\text{cryst}})^{2/3} \quad (10)$$

Then, taking  $\gamma_{\text{quartz}}$  equal to  $4.44 \text{ J.m}^{-2}$ , one obtained  $\gamma_{\text{SiO}_2} = 4 \text{ J.m}^{-2}$ , which further gives a fracture toughness of  $0.76 \text{ MPa} \cdot \sqrt{\text{m}}$ . This latter value is in agreement with the experimental value of  $0.8 \text{ MPa} \cdot \sqrt{\text{m}}$  obtained for a-SiO<sub>2</sub> in a dry environment.<sup>55)</sup> Again, the agreement between the theoretical and experimental values of  $\gamma$  for glasses from various chemical systems corroborate the assumption that the crack front opening displacement is within the interatomic distance, and fracture is purely elastic.

The experimental data presented in **Fig. 7** show that as far as non-metallic inorganic glasses are concerned,  $K_{Ic}$  and  $\gamma$  range typically from  $0.1$  to  $1.5 \text{ MPa} \cdot \sqrt{\text{m}}$  and from  $0.5$  to  $8 \text{ J.m}^{-2}$  respectively. Most brittle glasses are from chalcogenide and lead-borate systems, which turn out to exhibit at the same time a relatively large atomic packing density and a relatively small interatomic bond strength. In contrast, silicon oxynitride and oxycarbide glass forming systems provide the toughest glasses. The situation is nevertheless different in these latter systems. In the case of silicon oxynitride glasses, the large  $K_{Ic}$  values are attributed to the efficient packing of strongly bonded atoms (these glasses are also the stiffest), whereas in the case of silicon oxycarbide, the resistance toward crack initiation is supposed to derive from the important 3D cross-linking of a network consisting of strong bonds, and on possible crack tip shielding phenomena as the crack meets the nanoscale cavities where the free volume concentrates.

## 4. Conclusion

Interatomic bonds are quite similar in crystallized and amorphous polymorphs. Nevertheless, the atomic bonding arrangement in space is different. In particular, the presence of free volume makes the volume density of bonds, and thus the density of energy, smaller in glasses. Therefore, elastic moduli, which are given in  $\text{J.m}^3$  (Pa), are usually smaller. Consequently, the bulk modulus of different polymorphs depends nearly linearly on the atomic packing density. In the case of glasses, the free volume content, or the atomic packing density has a tremendous influence

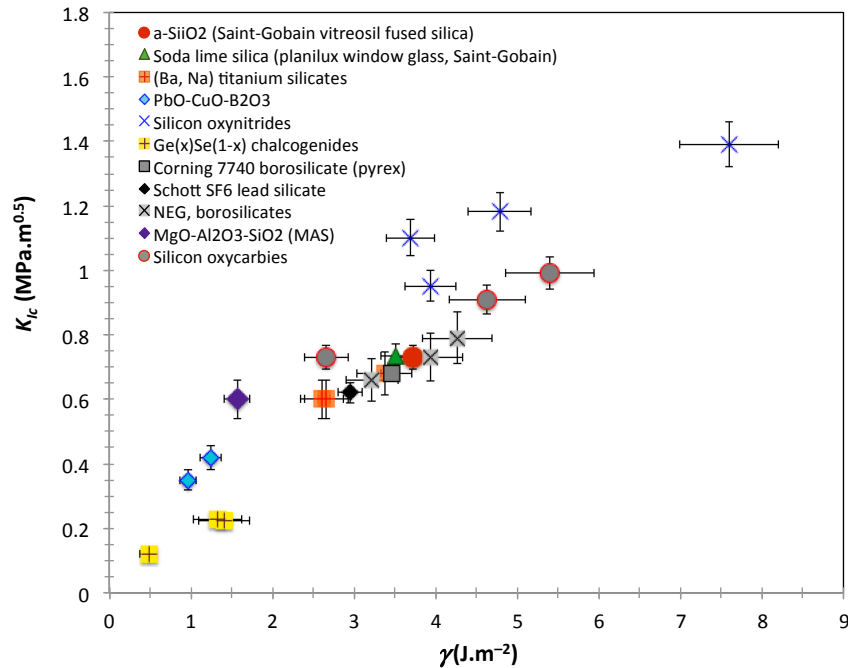


Fig. 7. Fracture toughness,  $K_{Ic}$ , as determined by means of self-consistent experimental techniques (*SEPB*, *CN* and *CSF*) and fracture surface energy, as derived from  $K_{Ic}$  and from the elastic moduli. Data were extracted from Ref. 54).

on the elastic moduli, and predominates over the bond strength in many cases. This is why silicon oxynitride glasses are much stiffer than their parent oxide glasses or why sodium aluminosilicate glasses are stiffer than sodium aluminoborate glasses although the Si–N bond is weaker than the Si–O one and the B–O bond strength is larger than the Si–O one.

However, as far as mechanical properties are concerned, it is important to distinguish phenomena occurring at the global scale such as volumetric change, and those occurring at some mesoscopic scale that are more heterogeneous in nature, such as shear-induced processes and fracture. These latter phenomena are mediated by the fine heterogeneous details of the atomic network (sliding and cleavage planes in crystals and easy shear paths in glass).

Hardness is intimately linked to a combination of contributing deformation mechanisms, including densification and shear processes. Therefore, it is a composite property involving both the global and the mesoscale at which shear localization occurs. The ease for dislocation glide in pure metals makes them relatively soft in comparison to metallic glasses, which are typically 15 times harder for a given shear modulus. Ionocovalent crystals are advantaged by a more efficient atomic packing than their amorphous polymorphs while the dislocation activity in these crystals is quite limited in ambient conditions. As a result, they are mostly (slightly) harder than their amorphous counterparts.

The intrinsic fracture surface energy ( $\gamma$ ) is intimately linked to the crack path. For “simple” mono-constituent glass such as a-SiO<sub>2</sub>, the experimental value for  $\gamma$  is in agreement with the prediction based on a random planar fracture path through the glass. In the case of multi-

component systems, it is necessary to account for the weakest links of the atomic network. Fracture toughness, as measured from a self-consistent method involving an atomically sharp crack ranges from 0.1 to 1.5 MPa $\cdot\sqrt{m}$  ( $\gamma$  is between 0.5 and 8 J $\cdot m^{-2}$ ), silicon oxynitride and oxycarbide glasses being the toughest among non-metallic inorganic glasses.

## References

- 1) P. K. Gupta and J. C. Mauro, *J. Chem. Phys.*, **130**, 094503 (2009).
- 2) J. C. Phillips, *J. Non-Cryst. Solids*, **34**, 153–181 (1979).
- 3) M. F. Thorpe, *J. Non-Cryst. Solids*, **57**, 355–370 (1983).
- 4) J. C. Maxwell, *Phil. Mag. and Journal of Science*, **27**, 250–261 (1864).
- 5) T. Rouxel, *J. Am. Ceram. Soc.*, **90**, 3019–3039 (2007).
- 6) G. N. Greaves, A. L. Greer, R. S. Lakes and T. Rouxel, *Nat. Mater.*, **10**, 823–837 (2011).
- 7) R. Limbach, A. Winterstein-Beckmann, J. Dellith, D. Möncke and L. Wondraczek, *J. Non-Cryst. Solids*, **417–418**, 15–27 (2015).
- 8) S. Striepe, N. Da, J. Deubener and L. Wondraczek, *J. Non-Cryst. Solids*, **358**, 1032–1037 (2012).
- 9) B. P. Rodrigues, C. Hühn, A. Erlebach, D. Mey, M. Sierka and L. Wondraczek, *Front. Mater.*, **4**, 20 (2017).
- 10) L. G. Liu, *Mech. Mater.*, **14**, 283–290 (1993).
- 11) K. Philipps, R. P. Stoffel, R. Dronskowski and R. Conrath, *Front. Mater.*, **4**, 2 (2007).
- 12) O. Shimomura, S. Minomura, N. Sakai, K. Asaumi and K. Tamura, *Philos. Mag.*, **29**, 547–558 (1974).
- 13) G. Demazeau, *Z. Naturforsch.*, **61b**, 799–807 (2006).
- 14) A. Makishima and J. D. Mackenzie, *J. Non-Cryst. Solids*, **12**, 35–45 (1973).
- 15) T. Rouxel and Y. Yokoyama, *J. Appl. Phys.*, **118**,

- 044901 (2015).
- 16) T. Rouxel, J. I. Jang and U. Ramamurty, *Prog. Mater. Sci.*, **121**, 10834 (2021).
- 17) E. Kulik, N. Nishiyama, Y. Higo, N. A. Gaida and T. Katsura, *J. Am. Ceram. Soc.*, **102**, 2251–2256 (2019).
- 18) D. L. Whitney, M. Broz and R. Cook, *Am. Mineral.*, **92**, 281–288 (2007).
- 19) F. M. Ernsberger, *J. Am. Ceram. Soc.*, **51**, 545–547 (1968).
- 20) K. W. Peter, *J. Non-Cryst. Solids*, **5**, 103–115 (1970).
- 21) A. Perriot, D. Vandembroucq, E. Barthel, V. Martinez, L. Grosvalet, C. Martinet and B. Champagnon, *J. Am. Ceram. Soc.*, **89**, 596–601 (2006).
- 22) S. Yoshida, J. C. Sangleboeuf and T. Rouxel, *J. Mater. Res.*, **20**, 3404–3412 (2005).
- 23) T. Rouxel, H. Ji, J. P. Guin, F. Augereau and B. Rufflé, *J. Appl. Phys.*, **107**, 094903 (2010).
- 24) W. H. Wang, C. Dong and C. H. Shek, *Mater. Sci. Eng.*, **R44**, 45–89 (2004).
- 25) J. P. Guin, T. Rouxel, J. C. Sangleboeuf, I. Melscoët and J. Lucas, *J. Am. Ceram. Soc.*, **85**, 1545–1552 (2002).
- 26) H. Lemercier, T. Rouxel, D. Fargeot, J. L. Besson and B. Piriou, *J. Non-Cryst. Solids*, **201**, 128–145 (1996).
- 27) P. Sellappan, A. Sharafat, V. Keryvin, P. Houizot, T. Rouxel, J. Grins and S. Esmailzadeh, *J. Non-Cryst. Solids*, **356**, 2120–2126 (2010).
- 28) T. Rouxel, J. C. Sangleboeuf, J. P. Guin, V. Keryvin and G. D. Sorarù, *J. Am. Ceram. Soc.*, **84**, 2220–2224 (2001).
- 29) P. Sellappan, T. Rouxel, F. Celarie, E. Becker, P. Houizot and R. Conradt, *Acta Mater.*, **61**, 5949–5965 (2013).
- 30) X. Jiang, J. Zhao and X. Jiang, *Comp. Mater. Sci.*, **50**, 2287–2290 (2011).
- 31) A. Kraych, P. Carrez and P. Cordier, *Earth Planet. Sc. Lett.*, **452**, 60–68 (2016).
- 32) “Dislocations in Solids”, Ed. by J. P. Hirth and L. Kubin, Elsevier Pub. (2010) Vol. 16.
- 33) J. C. Doukhan and L. Trépiéd, *B. Mineral.*, **108**, 97–123 (1985).
- 34) T. Masuda, T. Hiraga, H. Ikei, H. Kanda, Y. Kugimiya and M. Akizuki, *Geophys. Res. Lett.*, **27**, 2773–2776 (2000).
- 35) C. R. Kurkjian, G. W. Kammlott and M. M. Chaudhri, *J. Am. Ceram. Soc.*, **78**, 737–744 (1995).
- 36) B. A. Proctor, I. Whitney and J. W. Johnson, *Proc. R. Soc. Lon. Ser.-A*, **297**, 534–557 (1967).
- 37) F. Yuan and L. Huang, *Sci. Rep.-UK*, **4**, 5035 (2014).
- 38) R. Lacroix, G. Kermouche, G. Teisseire and E. Barthel, *Acta Mater.*, **60**, 5555–5566 (2012).
- 39) W. Pabst and E. Gregorova, *Ceram-Silikaty*, **57**, 167–184 (2013).
- 40) D. J. Weidner and H. R. Carleton, *J. Geophys. Res.*, **82**, 1334–1446 (1977).
- 41) C. S. Zha, R. J. Hemley, H. K. Mao, T. S. Duffy and C. Meade, *Phys. Rev. B*, **50**, 13105–13111 (1994).
- 42) T. Rouxel, *Philos. T. Roy. Soc. A*, **373**, 20140140 (2015).
- 43) M. Wada, H. Furukawa and K. Fujita, *Proc. X Int. Congr. Glass*, **11**, 39–46 (1974).
- 44) Y. Kato, H. Yamazaki, S. Yoshida and J. Matsuoka, *J. Non-Cryst. Solids*, **356**, 1768–1773 (2010).
- 45) I. Hasdemir, S. Striepe, J. Deubener and K. Simon, *J. Non-Cryst. Solids*, **408**, 51–56 (2015).
- 46) C. Hermansen, J. Matsuoka, S. Yoshida, H. Yamazaki, Y. Kato and Y. Z. Yue, *J. Non-Cryst. Solids*, **364**, 40–43 (2013).
- 47) S. Yoshida, *J. Non-Cryst. Solids*, **X**, 1, 100009 (2019).
- 48) T. Rouxel and S. Yoshida, *J. Am. Ceram. Soc.*, **1**, 1–23 (2017).
- 49) B. R. Lawn, B. J. Hockey and S. M. Wiederhorn, *J. Mater. Sci.*, **15**, 1207–1223 (1980).
- 50) H. Tanaka, Y. Bando, Y. Inomata and M. Mitomo, *J. Am. Ceram. Soc.*, **71**, C-32–C-33 (1988).
- 51) S. Wang, Z. Qin, G. S. Jung, F. J. Martin-Martinez, K. Zhang, M. J. Buehler and J. H. Warner, *ACS Nano*, **10**, 9831–9839 (2016).
- 52) Link to the lattice parameters of the  $\alpha$  quartz crystal: <http://www.librairiedemolecules.education.fr/outils/minus/app/minus.htm#>.
- 53) M. Iwasa and R. C. Bradt, *Mater. Res. Bull.*, **22**, 1241–1248 (1987).
- 54) T. Rouxel, *Scripta Mater.*, **137**, 109–113 (2017).
- 55) S. M. Wiederhorn, *J. Am. Ceram. Soc.*, **52**, 99–105 (1969).